Research Square

Preprints are preliminary reports that have not undergone peer review.
They should not be considered conclusive, used to inform clinical practice,
or referenced by the media as validated information.

Blood-Testis Barrier-Targeted DNA Nanomedicine for Fertility Preservation During Prepubertal Cisplatin Chemotherapy

Qiwei Chen
Zhujiang Hospital
Zijie Fang
Zhujiang Hospital
Kaixuan Guo
Zhujiang Hospital
Chengyu Feng
Zhujiang Hospital
Junke Liang
Zhujiang Hospital
Jieleng Huang
Guangdong Provincial People's Hospital
Lihua Yu
Zhujiang Hospital
Feng Zhao
Nanjing First Hospital
Shuxian Wang
Nanjing Medical University
Abai Xu
lc96xab@163.com

Zhujiang Hospital

Research Article

Keywords: Tetrahedral framework nucleic acids, blood-testis barrier, GS24 aptamer, DNA nanotechnology, targeted drug delivery

Posted Date: November 24th, 2026

DOI: https://doi.org/10.21203/rs.3.rs-11677065/v1

License: This work is licensed under a Creative Commons Attribution 4.0 International License.
Read Full License

Additional Declarations: No competing interests reported.

Blood-Testis Barrier-Targeted DNA Nanomedicine for Fertility Preservation During Prepubertal Cisplatin Chemotherapy

Qiwei Chen[1,†], *Zijie Fang*[1,†], *Kaixuan Guo*[1,†], *Chengyu Feng*[2,†], *Junke Liang*[1], *Jieleng Huang*[3], *Lihua Yu*[1], *Feng Zhao*[4,*], *Shuxian Wang*[5,*] *and Abai Xu*[1,*]

[†]These authors contributed equally to this work.

*Corresponding author

E-mails:

urojames@163.com (Feng Zhao)

wsxnju95@163.com (Shuxian Wang)

lc96xab@163.com (Abai Xu)

Abstract

Cisplatin-based chemotherapy in prepubertal males causes irreversible blood-testis barrier (BTB) damage and permanent infertility, yet no clinically viable fertility preservation strategy exists so far. Herein, a transcriptome-guided, BTB-targeted nanomedicine platform is developed by functionalizing tetrahedral framework nucleic acids (tFNAs) with the GS24 DNA aptamer—a high-affinity ligand for transferrin receptor (TfR) constitutively expressed on BTB vascular endothelium. Three size-tunable tFNAs (3.4, 8.1, 10.2 nm) and their GS24-conjugated counterparts (tFNAs-GS; 13, 18, 21.4 nm) are synthesized, respectively. Systematic *in vivo* organ distribution studies reveal that the small-sized tFNAs-GS (13 nm) exhibits superior testicular enrichment in a size-dependent manner ($P < 0.01$). Transcriptomic profiling of cisplatin-injured TM4 Sertoli cells identifies Krt16 as the most significantly upregulated gene and the integrated stress response (ISR) pathway as the key pathologically activated signaling cascade. ISRIB, a small-molecule ISR inhibitor, is physically loaded onto (S)tFNAs-GS to construct ISRIB@(S)tFNAs-GS (13.2 nm). This nanoplatform demonstrates excellent serum stability (24 h), potent BTB-targeting capability, and significant protective effects both *in vitro* and *in vivo*—restoring tight junction gene expression, suppressing Krt16 upregulation, reducing BTB permeability, and preserving seminiferous tubule architecture. This work establishes a DNA nanotechnology paradigm for chemotherapy-associated reproductive protection, addressing the long-standing clinical challenge of prepubertal fertility preservation.

Keywords: Tetrahedral framework nucleic acids; blood-testis barrier; GS24 aptamer; DNA nanotechnology; targeted drug delivery

1. Introduction

Childhood cancer remains a substantial global health burden, accounting for 1-4% of all human cancers worldwide, with nearly 400,000 new pediatric cases diagnosed annually[1,2]. Advances in multimodal chemotherapy and standardized supportive care have increased the 5-year survival rate of childhood cancer to more than 85% in developed countries, transforming once-fatal cancers diagnoses into manageable chronic conditions[2]. In China, the overall 5-year survival rate among children and adolescents with cancer has reached 77.2%, with rates exceeding 80% for several major cancer types[3]. As the number of childhood cancer survivors continues to grow, long-term adverse sequelae of anticancer therapy complications have become an increasingly important clinical concern. More than two-thirds of childhood cancer survivors experience at least one irreversible complication associated with chemotherapy or radiotherapy[4]. Among these sequelae, chemotherapy-induced male infertility severely impairs reproductive health, psychological well-being, and long-term quality of life, which is a core research focus at the intersection of pediatric oncology and reproductive medicine.

Cisplatin, a the first platinum-containing alkylating agent, remains the cornerstone of pediatric oncology treatment regimens for malignancies including hepatoblastoma, germ cell tumors, osteosarcoma, and neuroblastoma[5-7]. Clinical follow-up studies have shown lower adult fertility rates among survivors exposed to cisplatin during childhood than among their healthy siblings, indicating severe long-term reproductive toxicity[8,9]. Mechanistically, cisplatin induces DNA cross-linking and apoptosis in testicular Sertoli cells, disrupts intracellular redox homeostasis and mitochondrial function, and promotes the accumulation of excessive reactive oxygen species (ROS)[10]. The prepubertal testis may be particularly susceptible to cisplatin toxicity because the blood-testis barrier (BTB), formed by tight junctions between adjacent Sertoli cells, is still undergoing maturation. Cisplatin can disrupt BTB integrity by downregulating key tight junction proteins including ZO-1 and claudin-1, thereby compromising the Sertoli cell barrier, depleting spermatogonial stem cells, and ultimately leading to persistent spermatogenic dysfunction and permanent male infertility[11].

Current clinical fertility preservation strategies for pediatric patients rely primarily on sperm cryopreservation, which requires mature spermatozoa and is therefore not applicable to prepubertal

boys who have not initiated spermatogenesis[12-14]. Although testicular tissue cryopreservation, with the prospect of subsequent autotransplantation, has been explored as an experimental alternative, its clinical application remains limited by concerns including potential contamination with malignant cells, unstable graft survival efficiency, and ethical controversy[15]. Given that spermatogonial stem cells in the prepubertal testis provide the cellular foundation for spermatogenesis throughout reproductive life, there is an urgent need to develop in situ pharmacological strategies to protect these cells during chemotherapy. However, insufficient accumulation of protective agents in testicular tissues due to the barrier function of the BTB remains a major technical obstacle to effective testicular protection. Conventional small-molecule protective agents are limited by non-specific systemic distribution, rapid metabolic clearance, and low testicular accumulation, resulting in limited therapeutic effects and potential systemic adverse effects.

DNA nanotechnology, pioneered by Seeman in 1982, has emerged as a powerful platform for programmable, biocompatible drug delivery[16-18]. Among DNA nanostructures, tetrahedral framework nucleic acids (tFNAs) have attracted particular attention owing to their structural rigidity, uniform size, ease of functionalization, high specific surface area, flexible drug loading, and inherent capacity to traverse biological barriers. tFNAs have demonstrated efficacy in delivering small molecules, nucleic acid therapeutics, and proteins across various disease models[16-19]. However, systemic administration of unmodified tFNAs results predominantly in hepatic and renal accumulation, with minimal testis targeting, highlighting the need for active targeting strategies to improve testicular drug delivery.

The transferrin receptor (TfR) is highly expressed on vascular endothelial cells associated with both the blood-brain barrier (BBB) and the BTB, two major blood-tissue barriers sharing several molecular features[20,21]. GS24, a 64-nucleotide DNA aptamer with high affinity for TfR on brain capillary endothelial cells, has been shown to enhance brain-targeted drug delivery across the BBB[20-23]. Given the TfR homology between BBB and BTB endothelium, we hypothesized that GS24 functionalization could confer testis-targeting capability on tFNAs, enabling BTB-specific drug delivery—an approach rarely investigated for testicular protection.

Existing studies on protection against cisplatin-induced testicular injury have mainly focused on natural plant extracts or empirical compound screening, with few investigations targeting specific

signaling pathways in Sertoli cells based on unbiased transcriptomic analysis. In this study, we innovatively combined DNA nanodelivery technology with a precision pathway-intervention strategy for prepubertal fertility preservation. We first constructed tFNAs of three different sizes and GS24-modified tFNAs-GS nanocarriers and screened for the optimal carrier with superior BTB-targeting efficiency via *in vitro* and *in vivo* biodistribution analyses. Subsequently, transcriptome sequencing of cisplatin-injured TM4 Sertoli cells was performed to identify key differentially expressed genes and aberrantly activated signaling pathways, and ISRIB, a highly specific small-molecule inhibitor of the integrated stress response (ISR) pathway, was selected as the protective agent[24-26]. A BTB-targeted ISRIB@(S)tFNAs-GS nanoplatform was then fabricated, and its protective effects and molecular mechanisms against cisplatin-induced testicular damage were comprehensively evaluated at cellular and animal levels.

This study presents three key innovations. First, it pioneers the application of GS24-modified tFNAs to facilitate targeted delivery in the prepubertal testis, addressing a long-standing clinical challenge in fertility preservation for prepubertal patients. Second, it systematically characterizes the size-dependent BTB-targeting performance of tFNAs-GS nanocarriers and identifies the ISR/Krt16 axis as a key regulatory mechanism underlying cisplatin-induced Sertoli cell injury via transcriptome profiling. Third, the constructed ISRIB@(S)tFNAs-GS nanosystem integrates favorable biosafety, precise targeting, and pathway-specific intervention, providing a potentially translatable strategy for pediatric reproductive protection. This study not only offers a novel approach to fertility preservation during prepubertal chemotherapy but also expands the application of framework nucleic acid nanomaterials in biological-barrier penetration and precision therapy **(Figure 1)**.

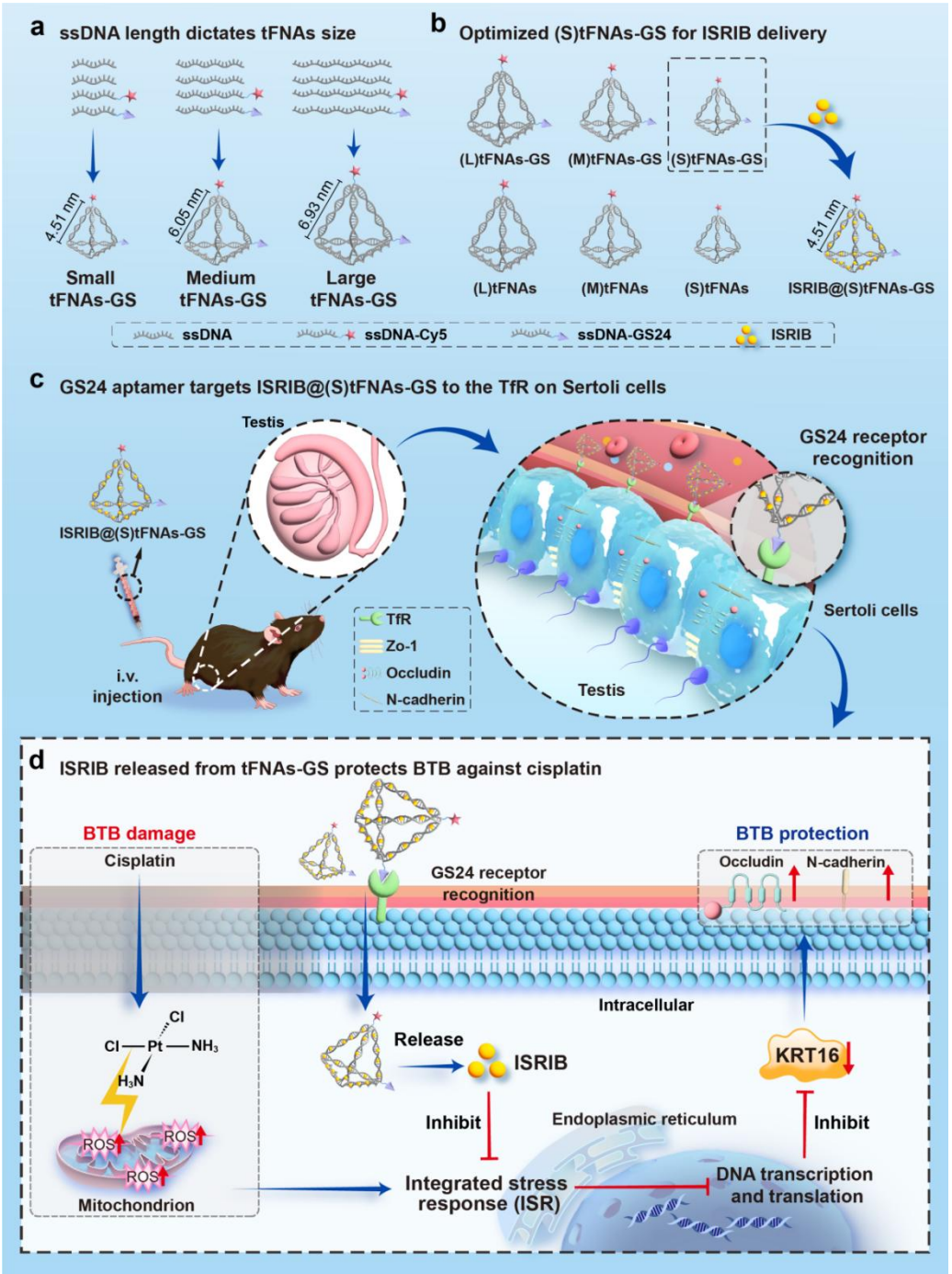


Figure 1. Schematic illustration of ISRIB@tFNAs-GS synthesis and its therapeutic mechanism against cisplatin-induced testicular injury. (a-b) Synthesis of the tetrahedral framework nucleic acid system and drug-loading platform *via* one-step thermal annealing. (c) GS24 aptamer confers testis-targeting capability on tFNAs *via* TfR-mediated BTB penetration. (d) ISRIB@tFNAs-GS protects against cisplatin-induced testicular injury by maintaining BTB integrity and suppressing ISR pathway activation, thereby preserving the spermatogenic microenvironment.

2. Results and Discussion

2.1. Construction and Characterization of Size-Tunable tFNAs and tFNAs-GS Nanoplatforms

Through rational variation of the lengths of the four constituent single-stranded DNAs (ssDNAs), three tFNAs with distinct sizes (small, medium, and large) were designed and self-assembled in a single thermal annealing step in Tris-Mg2+ buffer (95 °C for 10 min, followed by 4 °C for 20 min). The GS24 aptamer was conjugated to the 5'-end of Strand 3 in each size variant to generate the corresponding tFNAs-GS constructs. Strand 1 was labeled with Cy5 for fluorescence tracking. All constructs were purified by ultrafiltration to remove unannealed ssDNA precursors. This one-step synthesis approach offers significant advantages over multi-step conjugation strategies, including high yield, structural uniformity, and batch-to-batch reproducibility, which are essential for translational applications.

The structural integrity and purity of the assembled nanostructures were evaluated by 8% non-denaturing polyacrylamide gel electrophoresis (PAGE). As shown in **Figure 2b-2j**, each tFNAs-GS construct displayed a single, discrete band with slower migration compared to the corresponding unmodified tFNAs, confirming successful GS24 conjugation and structural homogeneity. Electrophoretic mobility decreased with increasing carrier size: small tFNAs, hereafter referred to as (S)tFNAs, migrated fastest, followed by medium tFNAs, hereafter referred to as (M)tFNAs, and large tFNAs, hereafter referred to as (L)tFNAs migrated slowest. After GS24 aptamer modification, all tFNAs-GS groups exhibited further reductions in electrophoretic mobility compared with their unmodified counterparts, attributed to the increased molecular weight and steric hindrance caused by GS24 conjugation.

Dynamic light scattering (DLS) analysis revealed narrow size distributions for all six constructs: (S)tFNAs (3.4 ± 0.3 nm), (S)tFNAs-GS (13.0 ± 1.2 nm), (M)tFNAs (8.1 ± 0.5 nm), (M)tFNAs-GS (18.0 ± 1.5 nm), (L)tFNAs (10.2 ± 0.7 nm), and (L)tFNAs-GS (21.4 ± 1.8 nm) **(Figure 2k)**. The approximately 5-11 nm increase in particle size following GS24 conjugation was consistent with the projected extension of the 64-nucleotide aptamer arm from the tetrahedral vertex. The uniform particle size and excellent dispersion of the synthesized nanosystems indicated successful assembly without aggregation—an important consideration for *in vivo* applications, as nanoparticle aggregation

may accelerate clearance and promote off-target accumulation.

Serum stability is an important prerequisite for the *in vivo* circulation and delivery efficacy of DNA nanocarriers. PAGE analysis showed that (S)tFNAs-GS maintained intact and uniform band morphology after incubation with 10% fetal bovine serum (FBS) at room temperature for 24 h, without obvious degradation or structural dissociation **(Figure S1)**. This robust serum stability, attributable to the rigid tetrahedral architecture and dense DNA packing, provides a physicochemical basis for subsequent *in vivo* systemic delivery. The negatively charged phosphate backbone and compact three-dimensional structure confer resistance to nuclease degradation, a well-established advantage of tFNAs over linear DNA counterparts[27].

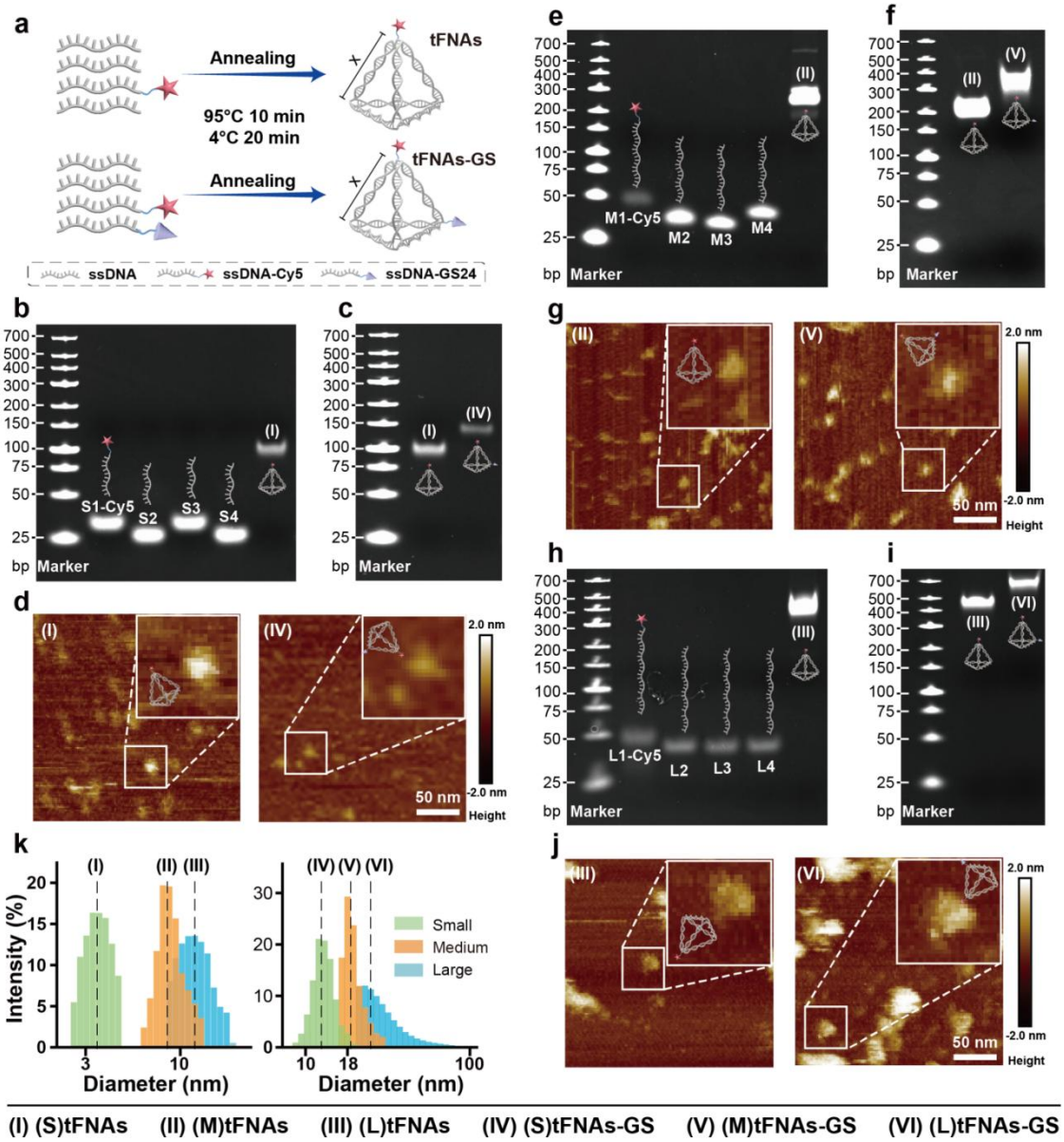


Figure 2. Construction and characterization of size-tunable tFNAs and tFNAs-GS nanoplatforms. (a) One-step preparation of size-tunable tFNAs and tFNAs-GS nanoplatforms. (b-c) PAGE analysis of (S)tFNAs and (S)tFNAs-GS, respectively. (d) AFM image of (S)tFNAs and (S)tFNAs-GS. Scale bar: 50 μm. (e-f) PAGE analysis of (M)tFNAs and (M)tFNAs-GS , respectively. (g) AFM image of (M)tFNAs and (M)tFNAs-GS. Scale bar: 50 μm. (h-i) PAGE analysis of (L)tFNAs and (L)tFNAs-GS respectively. (j) AFM image of (S)tFNAs and (S)tFNAs-GS. Scale bar: 50 μm. (k) DLS size distribution profiles of all six constructs, demonstrating narrow polydispersity and uniform hydrodynamic diameters.

2.2. In Vitro Cellular Uptake and Size-Dependent Internalization

Before proceeding to *in vivo* evaluation, the cellular uptake of the three sizes of tFNAs and tFNAs-GS was assessed *in vitro*. TM4 cells were incubated with Cy5-labeled constructs (100 nM) for 5, 30, and 60 mins, followed by confocal laser scanning microscopy (CLSM) and quantitative fluorescence analysis. All six constructs were readily internalized, with Cy5 fluorescence detectable as early as 5 mins and increasing in a time-dependent manner. Among the six constructs, (S)tFNAs-GS exhibited the most rapid and intense intracellular fluorescence, suggesting that smaller tetrahedral nanostructures facilitate more efficient cellular internalization **(Figure 3)**.

This size-dependent uptake pattern is consistent with previous reports that the cellular internalization of DNA tetrahedra is influenced by particle size and can involve clathrin-mediated endocytosis and caveolae-mediated pathways[28,29]. The enhanced cellular uptake of (S)tFNAs-GS provided the initial rationale for prioritizing the small-sized platform in subsequent *in vivo* studies. Importantly, GS24 modification did not significantly impair cellular internalization compared to unmodified tFNAs, indicating that the aptamer conjugation at the tetrahedral vertex preserved the cell-penetrating capability of the nanostructure while introducing targeting functionality.

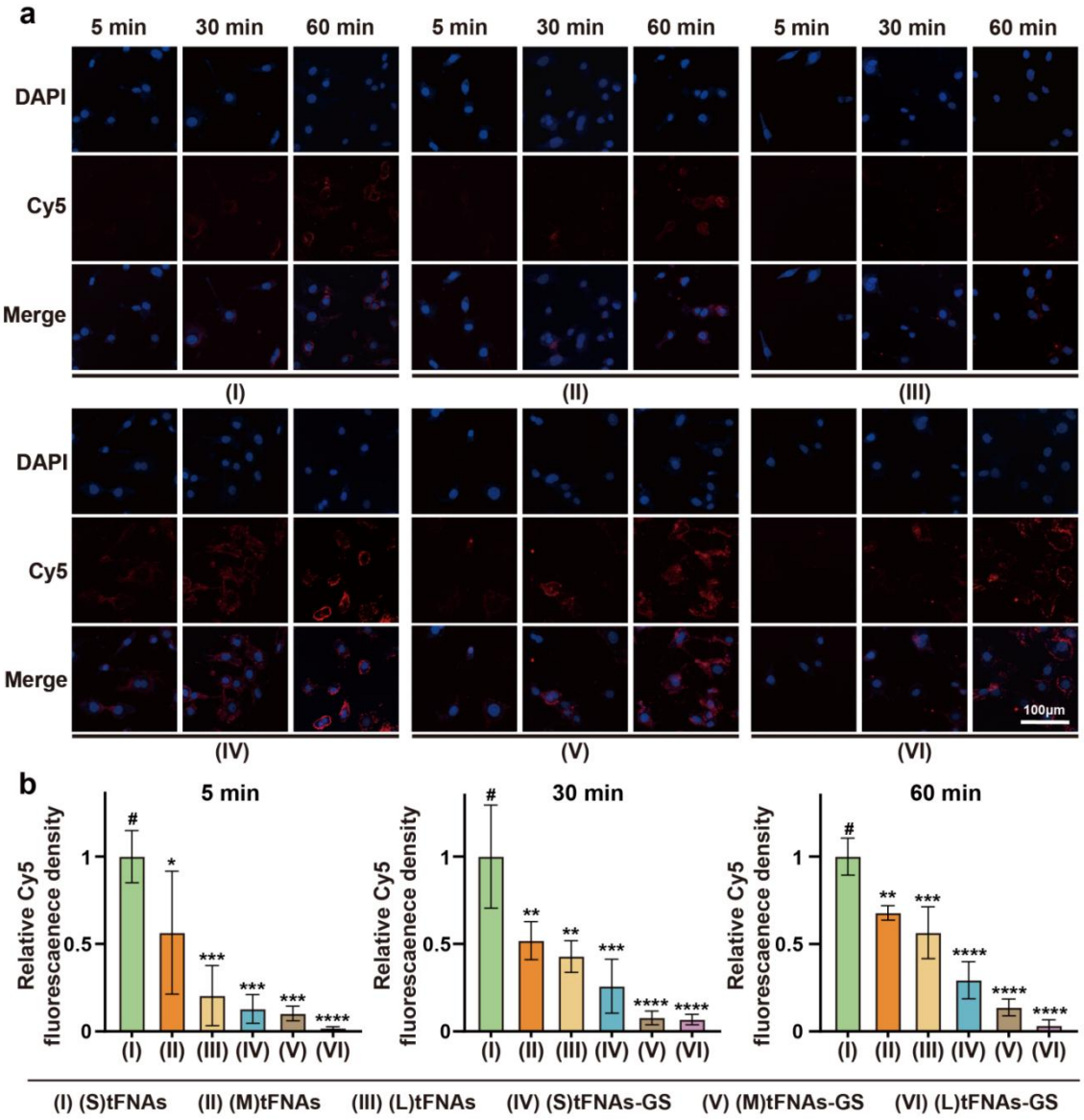


Figure 3. In vitro cellular uptake and size-dependent internalization of tFNAs and tFNAs-GS. (a) CLSM images of TM4 cells incubated with Cy5-labeled constructs (100 nM) for 5, 30, and 60 mins. Cell nuclei were stained with DAPI (blue) and the nanostructures were labeled with Cy5 (red). (b) Quantitative fluorescence analysis of relative Cy5 fluorescence density in TM4 cells at 5, 30, and 60 mins. # for comparisons between groups, **P < 0.01, ***P < 0.001, ****P < 0.0001.

2.3. Size-Dependent Testis Targeting and BTB Penetration of tFNAs-GS Nanocarriers

To systematically evaluate the *in vivo* biodistribution and testis targeting capability of tFNAs and tFNAs-GS nanocarriers of different sizes, IVIS Spectrum *in vivo* fluorescence imaging was performed on major organs 15 min after tail vein injection **(Figure 4a)**. Seven groups of 6–8-week-old male C57BL/6j mice (n = 5 per group) received tail vein injections of Cy5-labeled tFNAs or tFNAs-GS constructs (10 μM/kg).

Consistent with the inherent biodistribution characteristics of framework nucleic acids, unmodified tFNAs accumulated predominantly in the liver and kidneys, with negligible fluorescence signals detected in testicular tissues. This hepatorenal accumulation pattern is characteristic of DNA nanostructures and has been attributed to reticuloendothelial system uptake and renal filtration[30,31]. In contrast, all GS24-modified tFNAs-GS groups exhibited significant testicular fluorescence enrichment, accompanied by reduced renal accumulation, indicating that GS24 aptamer modification conferred BTB targeting ability on tFNAs and markedly altered their *in vivo* biodistribution.

Notably, testicular enrichment showed a pronounced size dependence. **Figure 4b** revealed that (S)tFNAs-GS (13 nm) achieved the highest testicular fluorescence intensity, while also showing the lowest renal retention—likely due to reduced renal filtration of the smaller, BTB-targeted construct. This size-dependent targeting performance may be related to the structural characteristics of the BTB, as tight-junction dimensions and transcytosis efficiency can influence the transport of nanoparticles across biological barriers[32]. (L)tFNAs-GS (21.4 nm) may experience greater steric hindrance and lower transcytosis efficiency, resulting in reduced testicular accumulation despite equivalent GS24-mediated TfR binding.

Confocal laser scanning microscopy of testicular cryosections further supported the IVIS findings **(Figure 4c)**. FITC administered 2 h before tFNAs-GS was used to visualize the BTB structure, while DAPI was used to stain cell nuclei. In mice treated with (S)tFNAs-GS, intense Cy5 signals (red) co-localized with FITC-labeled BTB (green), indicating specific BTB accumulation **(Figure 4d)**. Among the tFNAs-GS groups, (S)tFNAs-GS showed the clearest BTB-associated signal, with greater fluorescence intensity and deeper tissue penetration compared with (M)tFNAs-GS and (L)tFNAs-GS groups. These results collectively demonstrate that the BTB targeting and penetration ability of tFNAs-GS nanocarriers is size-dependent, with small-sized (S)tFNAs-GS showing the most favorable testis targeting performance. Therefore, (S)tFNAs-GS was selected as the preferred delivery platform for subsequent drug-loading and protective studies.

The observed size-dependent targeting can be attributed to the TfR-mediated transcytosis pathway. TfR is highly expressed on BTB endothelial cells, and upon GS24-mediated binding, the tFNAs-GS nanoparticles undergo receptor-mediated endocytosis followed by transcytosis across the endothelial monolayer[33]. (S)tFNAs-GS exhibited higher transport efficiency due to reduced

endosomal sorting complexity and more rapid exocytosis kinetics. These findings suggest that nanoparticle size is an important design consideration for BTB-targeted nanocarriers and may influence the efficiency of testicular drug delivery.

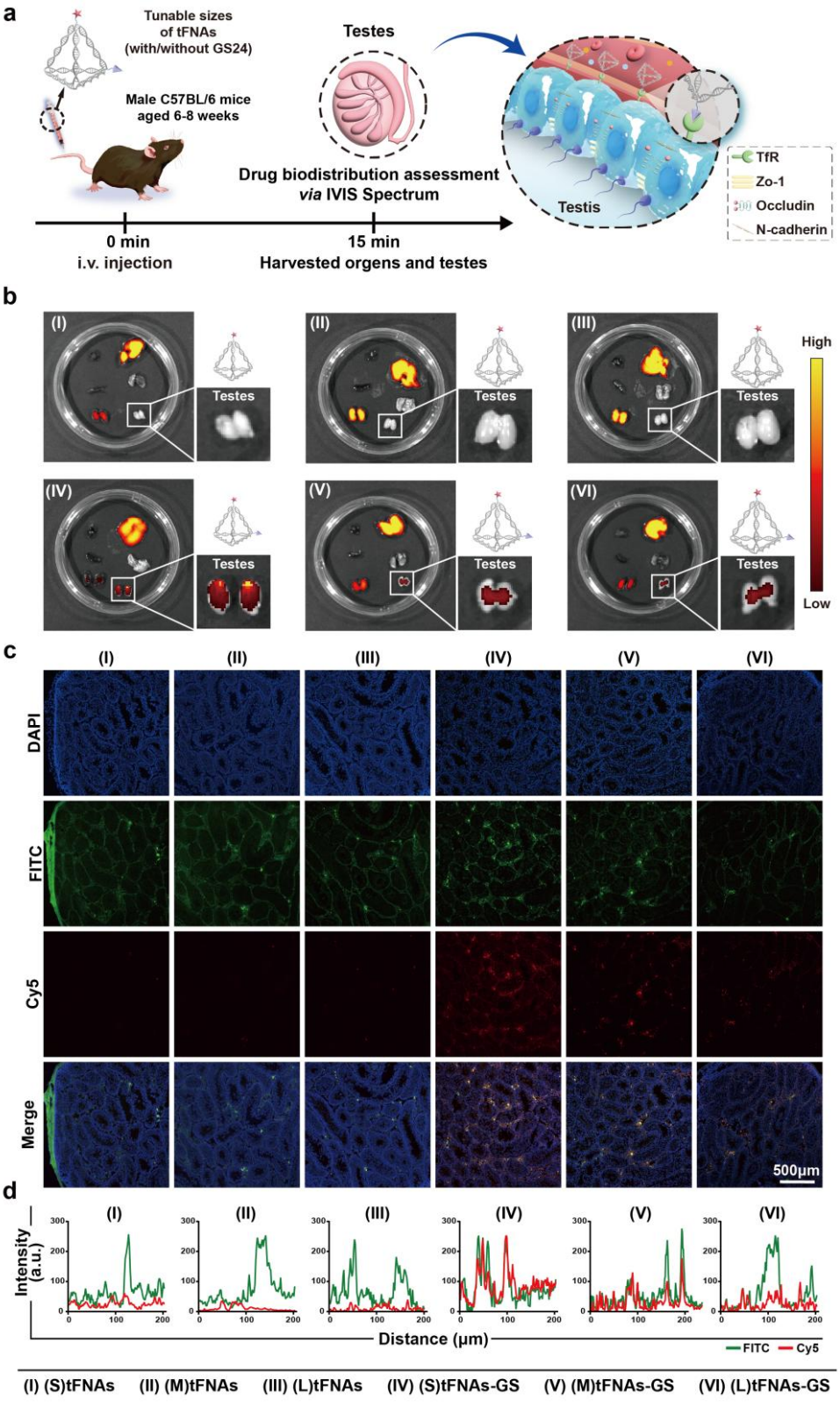


Figure 4. Testis targeting performance of size-tunable tFNAs and tFNAs-GS nanoplatforms. (a) Schematic of GS24-mediated BTB targeting via TfR. (b) *Ex vivo* organ fluorescence imaging (heart, liver, spleen, lung, kidney and testis) at 15 min post-injection. (c) Confocal fluorescence images of testicular cryosections showing FITC-labeled BTB (green), Cy5-labeled nanoplatform (red), and DAPI nuclei (blue). (d) Quantitative analysis of FITC/Cy5 signal ratios in treated biofilms.

2.4. Establishment and Characterization of Cisplatin-Induced Testicular Injury Model

To establish a clinically relevant injury model for subsequent mechanistic and therapeutic studies, cisplatin cytotoxicity was first evaluated in two mouse testicular cell lines: TM4 (Sertoli cells) and GC2 (spermatocytes). CCK-8 assays performed across a concentration gradient (0–0.192 mg/mL, 24 h) revealed that TM4 cells were markedly more sensitive to cisplatin (IC50 = 0.00284 ± 0.00046 mg/mL) than GC2 cells (IC50 = 0.01607 ± 0.00365 mg/mL). This differential sensitivity is biologically significant because Sertoli cells are key structural and functional constituents of the BTB and act as the first line of cellular defense against testicular toxicants. Their higher sensitivity to cisplatin suggests that Sertoli cell damage may contribute substantially to cisplatin-induced testicular toxicity[34]. Based on this cytotoxicity profiling, 0.003 mg/mL cisplatin was used in all subsequent *in vitro* experiments.

For the *in vivo* model, 6-week-old male C57BL/6j mice received intraperitoneal injections of cisplatin at 0, 1, 2.5, or 5 mg/kg daily for 3 consecutive days. Mice in the 5 mg/kg group exhibited the most pronounced phenotypic changes, including significant body weight loss (≈20.2%), marked lethargy, and poor grooming, while lower doses produced proportionally milder effects. RT-qPCR analysis of testicular tissue revealed dose-dependent downregulation of BTB tight junction genes: TJP1 (encoding ZO-1) and CLDN1 (encoding claudin-1) decreased progressively with increasing cisplatin doses ($P < 0.05$ at 2.5 and 5 mg/kg vs. control), while OCLN (encoding occludin) showed no significant change, likely due to its low basal expression in prepubertal testes. The differential responses of these tight-junction components to cisplatin are consistent with previous reports suggesting that ZO-1 and claudin-1 are more susceptible to stress-induced disruption due to their dynamic association with the actin cytoskeleton[35].

BTB integrity was further assessed using the FITC tracer assay. In control mice, FITC fluorescence was confined to the interstitial space and vasculature, with no detectable penetration into

the seminiferous tubules **(Figure S2)**. Cisplatin treatment resulted in a dose-dependent increase in FITC leakage into the tubular lumen, with the most extensive permeation observed at 5 mg/kg, indicating progressive disruption of BTB integrity. H&E staining of testicular tissues confirmed that moderate-dose cisplatin treatment successfully induced significant BTB disruption and testicular structural damage, mimicking the clinical prepubertal chemotherapy reproductive injury phenotype. Based on the combined considerations of animal tolerability and significant, quantifiable BTB damage, 5 mg/kg cisplatin was selected as the injury dose for all subsequent intervention studies.

2.5. Transcriptomic Profiling Identifies the ISR Pathway as a Potential Therapeutic Target

To elucidate the molecular mechanisms underlying cisplatin-induced Sertoli cell damage and identify potential protective targets, RNA-seq transcriptomic analysis was performed on TM4 cells treated with cisplatin (0.003 mg/mL, 24 h) and untreated controls (n = 3 biological replicates per group). This unbiased approach offers advantages over candidate-gene studies by enabling comprehensive pathway exploration without prior assumptions. Principal component analysis (PCA) revealed complete separation along PC1 (99.33% variance explained) of the two groups, with tight intra-group clustering, indicating robust model construction and data reliability **(Figure 5b)**.

Differential expression analysis ($|\log_2 FC| \geq 1$, $q < 0.05$) identified 6,214 differentially expressed genes (DEGs), including 2,918 upregulated and 3,296 downregulated **(Figure 5c)**. To validate the sequencing results, the seven most highly upregulated genes ($\log_2 FC \geq 8$)—Krt16, Gsdma3, Ptprcap, Gjc2, Gm29797, Ifnz and Etv2—were selected for RT-qPCR validation in both cell (TM4) and testicular tissue models. All seven genes showed significant upregulation consistent with sequencing trends, with Krt16 exhibiting the most pronounced and stable increase **(Figure 5d)**, establishing it as a potential biomarker for cisplatin-induced Sertoli cell injury. The marked upregulation of Krt16 (log2 FC > 10) further suggests a central role in the cellular stress response to cisplatin.

Gene Ontology (GO) and KEGG pathway enrichment analyses of the 2,918 upregulated genes revealed striking convergence on integrated stress response (ISR)-associated biological processes **(Figure 5e, 5f)**. The top 30 GO terms included unfolded protein response (UPR), response to oxidative stress, apoptotic regulation, kinase activation, protein phosphorylation, and protein ubiquitination—collectively accounting for more than 50% of the enriched terms. KEGG analysis

285 further confirmed significant enrichment in protein translation regulation, oxidative phosphorylation,
286 mitophagy, and spliceosome pathways, all functionally linked to ISR signaling. Notably, Krt16 has
287 been reported to be an ATF4-regulated component of the ISR, and key ISR effectors including Atf3,
288 Ddit3 (CHOP), and Ppp1r15a (GADD34) were among the upregulated DEGs[36].

289 The ISR is a key adaptive stress-response pathway in mammalian cells that integrates signals
290 from four stress-sensing kinases—PERK, GCN2, PKR and HRI—which converge on
291 phosphorylation of eukaryotic translation initiation factor 2α (eIF2α)[37]. This phosphorylation
292 process reduces global protein synthesis while selectively upregulating stress-responsive genes
293 including ATF4, CHOP, and GADD34. In the context of cisplatin-induced Sertoli cell injury,
294 sustained ISR activation leads to cellular dysfunction, tight junction damage, and tissue
295 microenvironment disorder. The transcriptomic findings of this study identify the ISR pathway as the
296 key pathologically activated cascade in cisplatin-induced Sertoli cell damage, providing a precise
297 therapeutic target for intervention. Based on these transcriptomic insights, ISRIB—a small-molecule
298 inhibitor that enhances eukaryotic initiation factor 2B (eIF2B) activity and reverses eIF2α
299 phosphorylation-mediated translational suppression, thereby blocking aberrant ISR activation—was
300 chosen as the protective agent. ISRIB has demonstrated efficacy in various stress-related disease
301 models, including traumatic brain injury, neurodegeneration, and chemotherapy-induced peripheral
302 neuropathy[38,39]. The selection of ISRIB is also supported by physicochemical properties, such as
303 low molecular weight and planar structure, which are favorable for tFNA loading and its established
304 safety profile in preclinical models. Importantly, unlike broad-spectrum cytoprotective agents, ISRIB
305 offers pathway-specific intervention that minimizes off-target effects—a critical advantage for
306 fertility preservation where systemic toxicity must be avoided.

307

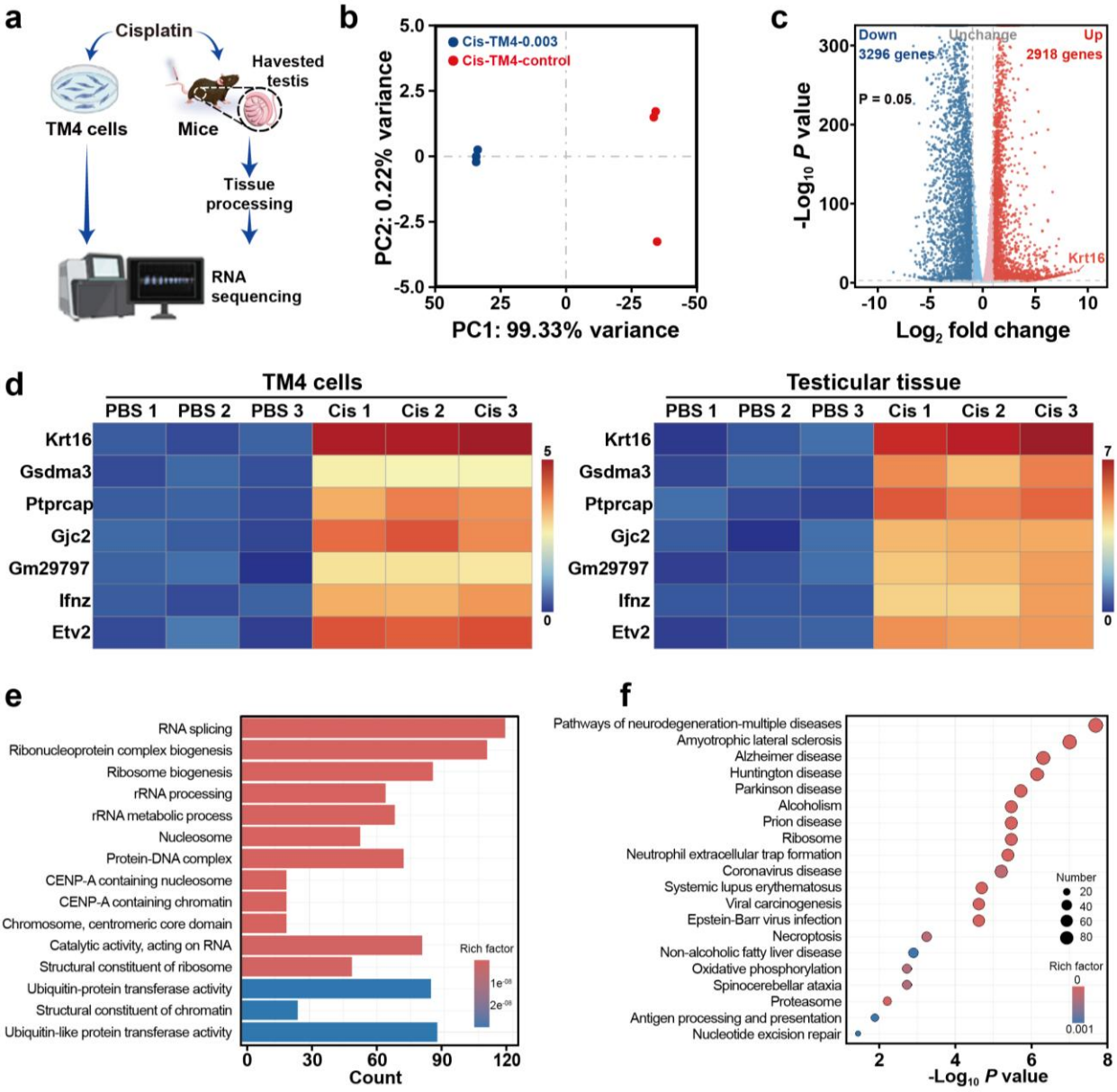


Figure 5. Transcriptomic analysis of cisplatin-injured TM4 cells and testicular tissue. (a) Schematic illustration of RNA-sequencing in TM4 cells and testicular tissue treated with cisplatin.(b) PCA showing clear separation between control and cisplatin groups in TM4 cells (n = 3 per group). (c) The volcano plot of differentially expressed genes in cisplatin-injured TM4 cells. (d) RT-qPCR validation of representative upregulated DEGs in cisplatin-injured TM4 cells and testicular tissue. (e-f) GO and KEGG enrichment analyses of upregulated DEGs, revealing convergence on ISR-associated biological processes.

2.6. Synthesis and Characterization of ISRIB@(S)tFNAs-GS

The ISRIB@(S)tFNAs-GS nanoplatform was constructed by co-incubating ISRIB with (S)tFNAs-GS at room temperature for 1–3 h, taking advantage of the physical loading capacity of the tFNA

architecture. The high specific surface area and negatively charged backbone of tFNAs facilitate electrostatic and hydrophobic interactions with small-molecule drugs, enabling efficient loading without covalent modification that could alter drug activity[40]. After loading, ultrafiltration was employed to remove unencapsulated free drug **(Figure 6a)**.

Successful assembly was verified using complementary techniques. An 8% PAGE analysis showed that ISRIB@(S)tFNAs-GS migrated to a position nearly identical to that of (S)tFNAs-GS **(Figure 6b)**—the negligible shift was attributable to the low molecular weight of ISRIB (≈ 300 Da) relative to the ≈ 30 kDa (S)tFNAs-GS scaffold. This migration pattern was consistent with physical loading rather than covalent conjugation, which would more significantly alter electrophoretic mobility. DLS analysis confirmed that drug loading only marginally increased the hydrodynamic diameter (13.2 ± 1.0 nm vs. 13.0 ± 1.2 nm for (S)tFNAs-GS), with no aggregation peaks **(Figure 6c, 6d)**, confirming uniform drug encapsulation without carrier disruption or drug precipitation. The encapsulation efficiency was determined by UV spectrophotometry and exceeded 85% at the optimal mass ratio.

Preservation of nanostructure integrity after drug loading is critical for maintaining BTB targeting and *in vivo* stability. Unlike conventional drug carriers that may undergo structural rearrangement upon drug loading, the rigid tetrahedral architecture of tFNAs provides mechanical stability that resists deformation[41]. This structural robustness ensures that GS24 aptamers remain accessible for TfR binding and that the nanoplatform retains its size-dependent penetration properties.

2.7. In Vitro Safety and Protective Efficacy of (S)tFNAs and ISRIB

Before constructing the combined nanoplatform, the biosafety and protective effects of (S)tFNAs and ISRIB were individually assessed in cisplatin-injured TM4 cells. This stepwise evaluation allowed the respective contributions of the carrier and drug to the final formulation to be assessed. CCK-8 cytotoxicity assays demonstrated that both (S)tFNAs (≤ 500 nM) and ISRIB (≤ 500 nM) maintained cell viability above 90–95%, with no significant difference from the control ($P > 0.05$), while concentrations of 1000 nM resulted in mild toxicity ($P < 0.01$) **(Figures S3, S4)**. These results established ≤ 500 nM as the safe working concentration range for both agents, providing a basis for subsequent combination studies **(Figure 6e, 6f)**.

In the protection assays, pre-treatment with either (S)tFNAs or ISRIB 1 h before cisplatin exposure improved TM4 cell viability. RT-qPCR analysis **(Figure 6g)** showed that both agents partially restored TJP1 and CLDN1 expression compared to cisplatin treatment alone and significantly suppressed cisplatin-induced Krt16 upregulation. The partial protective effect of (S)tFNAs alone is consistent with the reported anti-inflammatory and cytoprotective properties of DNA nanostructures, including their ability to scavenge reactive oxygen species and modulate cellular stress responses[42,43]. ISRIB (200 nM) exhibited greater protective effects than (S)tFNAs, consistent with its targeted inhibition of the ISR pathway. Based on the combined safety and efficacy profiles, 100 nM (S)tFNAs and 200 nM ISRIB were selected for subsequent combination studies.

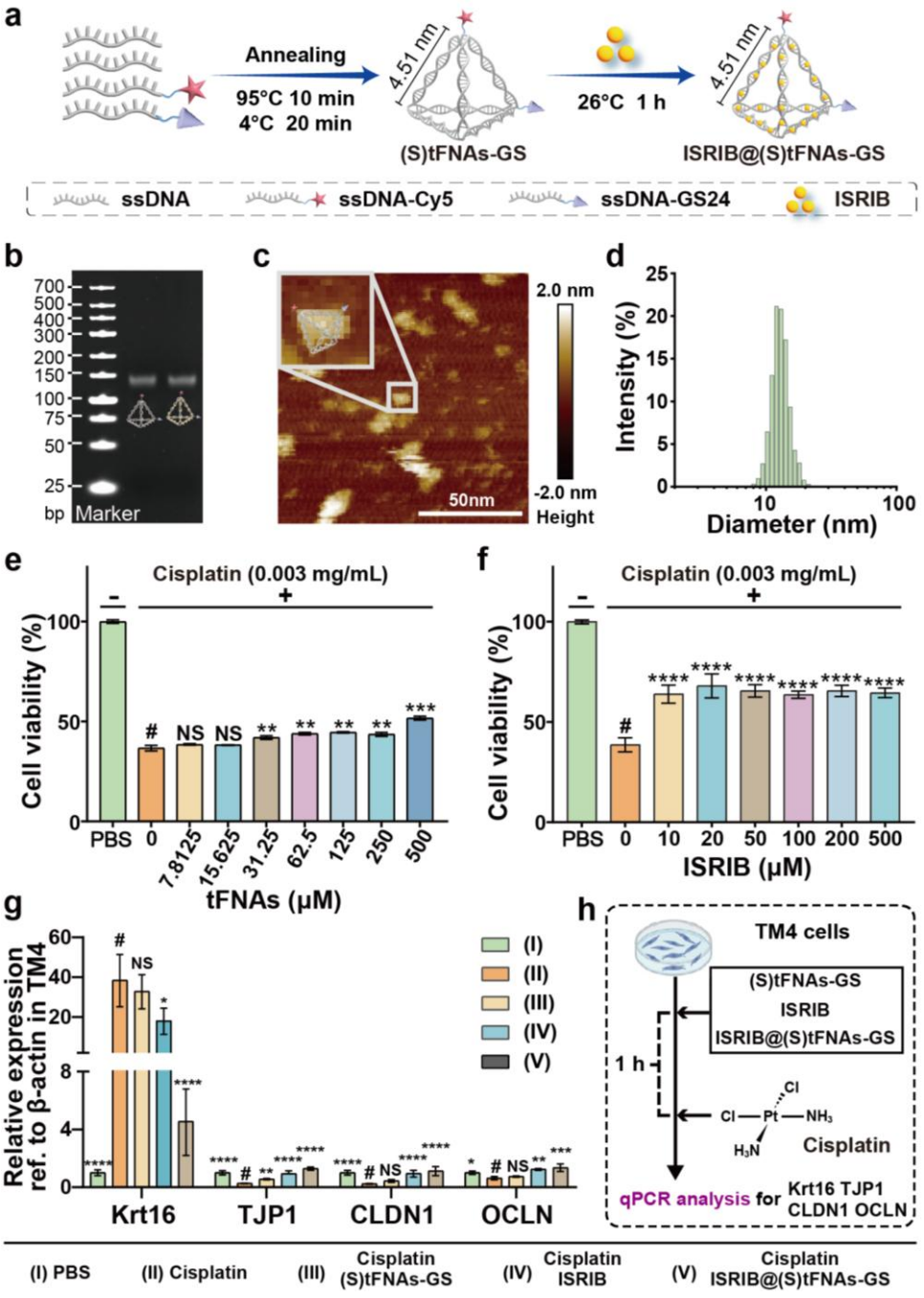


Figure 6. ***In vitro*** **assessment of ISRIB@(S)tFNAs-GS for biosafety and protective efficacy against cisplatin-induced testicular injury.** (a) Schematic of nanoplatform assembly *via* physical loading of ISRIB@(S)tFNAs-GS. (b) PAGE analysis of (S)tFNAs-GS and ISRIB@(S)tFNAs-GS verification of successful assembly. (c) AFM image of ISRIB@(S)tFNAs-GS. Scale bar: 100 μm. (d) DLS size distribution of ISRIB@(S)tFNAs-GS, confirming its uniform nanostructure. (e-f) *In vitro* biosafety evaluation of ISRIB and (S)tFNAs-GS across concentrations. (g-h) RT-qPCR and western blot analysis of BTB tight junction genes (Krt16, TJP1, CLDN1 and OCLN) in TM4 cells after different treatments. # for comparisons between groups, NS: no significant, **P < 0.01, ***P < 0.001.

2.8. In Vivo Protective Efficacy of ISRIB@(S)tFNAs-GS Against Cisplatin-Induced Testicular Injury

To evaluate the *in vivo* protective efficacy of the nanoplatform, 6-week-old male C57BL/6j mice were randomized into five groups (n = 5 per group): (1) Control (vehicle), (2) Cisplatin (5 mg/kg, i.p., days 1–3), (3) Cisplatin + ISRIB (free drug, i.p.), (4) Cisplatin + (S)tFNAs-GS (i.v.), and (5) Cisplatin + ISRIB@(S)tFNAs-GS (i.v.). The treatment protocol and timeline are illustrated in **Figure 7a**. Nanoplatforms or free drug were administered 15 min before each cisplatin injection to ensure the presence of the protective agents at the target sites before cisplatin exposure.

Body weight was monitored as a general indicator of cisplatin toxicity and treatment response **(Figure 7b)**. The control group exhibited normal weight gain (+4.5%), whereas the cisplatin-only group showed severe weight loss (-20.2%). The three intervention groups showed varying degrees of improvement: (S)tFNAs-GS modestly attenuated weight loss (-17.8%), free ISRIB provided moderate protection (-15.7%), and ISRIB@(S)tFNAs-GS produced the greatest attenuation of weight loss (-9.5%)—representing significant improvement (over 2-fold) compared to cisplatin alone and approximately 1.6- to 1.7-fold improvement compared to the other intervention groups. This superior efficacy underscores the benefit of targeted delivery: by concentrating ISRIB at the BTB, the nanoplatform achieves higher local drug concentrations while minimizing systemic exposure and associated off-target effects. The partial protection observed with free ISRIB at 5 mg/kg dose is consistent with its limited testicular accumulation due to BTB barrier function, highlighting the necessity of targeted delivery for effective testicular protection.

RT-qPCR analysis of testicular tissues **(Figure 7c)** showed that cisplatin significantly downregulated TJP1 ($P < 0.001$ vs. control), consistent with BTB disruption. All three interventions restored TJP1 expression to varying degrees, with ISRIB@(S)tFNAs-GS achieving the most significant recovery ($P < 0.05$ vs. cisplatin group). CLDN1 showed a similar restoration pattern. Notably, Krt16—the most highly upregulated gene identified in the transcriptomic screen—was significantly suppressed by both free ISRIB and ISRIB@(S)tFNAs-GS, with the nanoplatform demonstrating superior inhibition ($P < 0.05$ vs. free ISRIB). These findings indicate that targeted ISRIB delivery more effectively reverses the molecular changes associated with cisplatin-induced Sertoli cell damage. The restoration of tight-junction gene expression at the transcriptional level

provides molecular evidence supporting the preservation of BTB integrity, consistent with a protective effect of ISR modulation against stress-induced junctional disruption.

FITC tracer assays combined with confocal imaging provided direct morphological evidence of BTB protection **(Figure 7d)**. In the cisplatin-only group, extensive FITC fluorescence penetrated the seminiferous tubule lumens, indicating severe barrier disruption. Free ISRIB and (S)tFNAs-GS each partially reduced FITC leakage, while ISRIB@(S)tFNAs-GS treatment markedly restored BTB integrity, with FITC fluorescence largely confined to the interstitial space, closely resembling the control pattern. These results demonstrate that the nanoplatform effectively preserves the barrier function of the BTB against cisplatin-induced injury. The greater protective effect of ISRIB@(S)tFNAs-GS compared with free ISRIB reflects the enhanced local drug concentration achieved through GS24-mediated targeting, which facilitates ISRIB delivery to BTB endothelial cells and Sertoli cells where it exerts its cytoprotective effects.

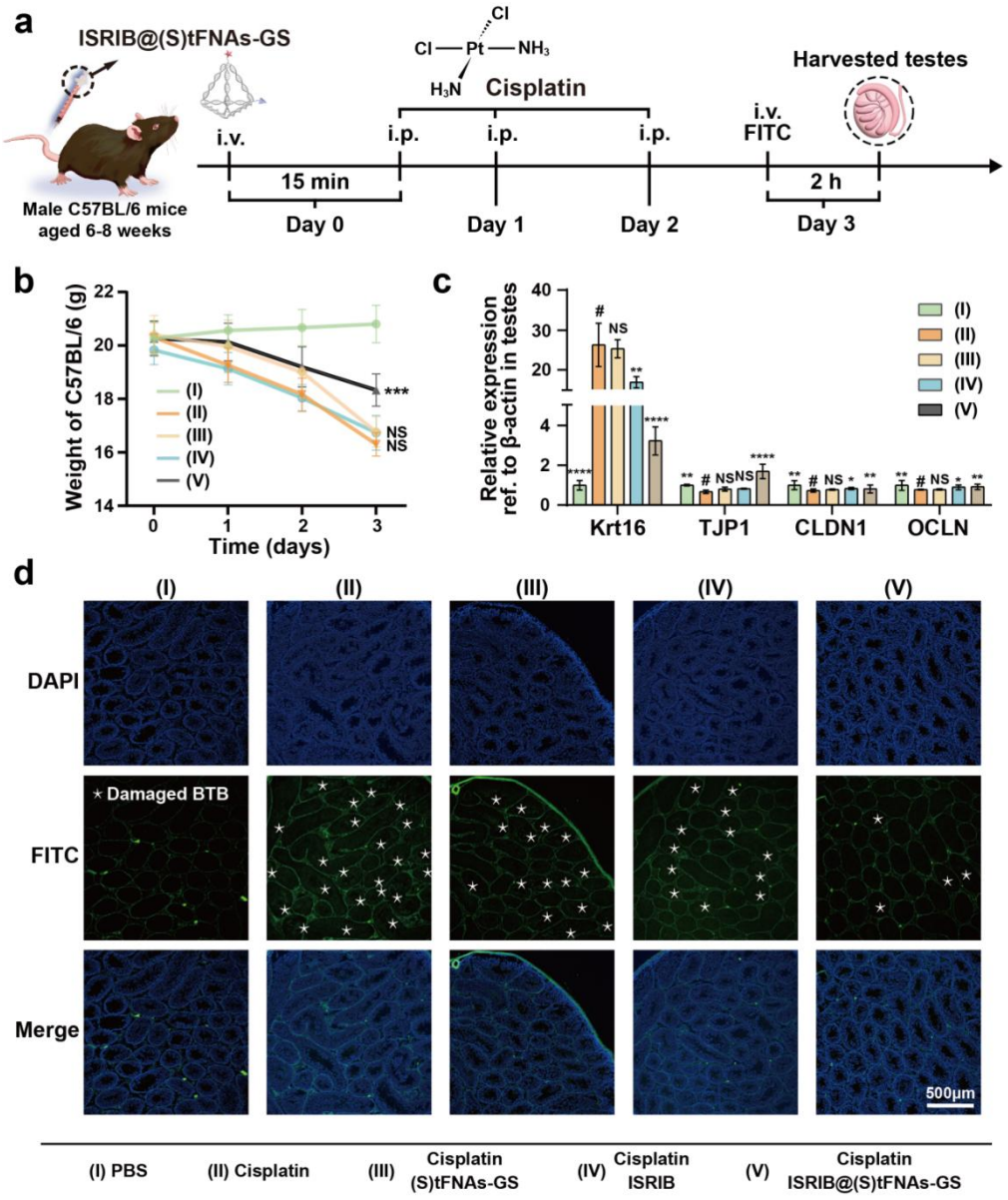


Figure 7. ***In vivo*** **assessment of ISRIB@(S)tFNAs-GS for protective efficacy against cisplatin-induced testicular injury.** (a) Mice received cisplatin (5 mg/kg, i.p.) on days 0-2, with nanoplatform administration 15 min before cisplatin injection on day 0. (b) Body weight changes of C57BL/6 treated with different groups (n = 5 per group). (c) RT-qPCR analysis of BTB tight junction genes (Krt16, TJP1, CLDN1 and OCLN) in testicular tissue after different treatments. (d-e) Confocal images (FITC-labeled) images of seminiferous tubule damage for assessment of the protective capacity of ISRIB@(S)tFNAs-GS after different treatments. # for comparisons between groups, NS: no significant, **P < 0.01, ***P < 0.001.

Hematoxylin and eosin (H&E) staining **(Figure 8a)** revealed that cisplatin treatment caused marked disorganization of seminiferous tubule architecture, including epithelial thinning, vacuolization, loss of regular tubular cross-sectional profile, and inflammatory infiltration. ISRIB@(S)tFNAs-GS treatment significantly ameliorated these structural abnormalities, maintaining

tubular integrity and epithelial thickness closer to those observed in the control group. Compared with the control, cisplatin treatment resulted in disrupted and patchy expression of ZO-1 and occludin (red triangles), with these tight-junction proteins failing to maintain their characteristic continuous linear pattern **(Figure 8b, 8c)**. Meanwhile, expression of the Sertoli cell cytoskeletal marker vimentin was significantly reduced **(Figure 8d)**. ISRIB@(S)tFNAs-GS administration successfully restored the expression and distribution of ZO-1, occludin, and vimentin, indicating a restorative effect on BTB integrity **(Figure 8e-8g)**. Both free ISRIB and (S)tFNAs-GS alone provided partial protection, whereas the targeted nanoplatform achieved the most pronounced histological preservation, consistent with the molecular and functional improvements observed. Preservation of seminiferous tubule architecture is functionally significant because the structural integrity of the seminiferous epithelium is essential for supporting spermatogonial stem cell proliferation and differentiation[44].

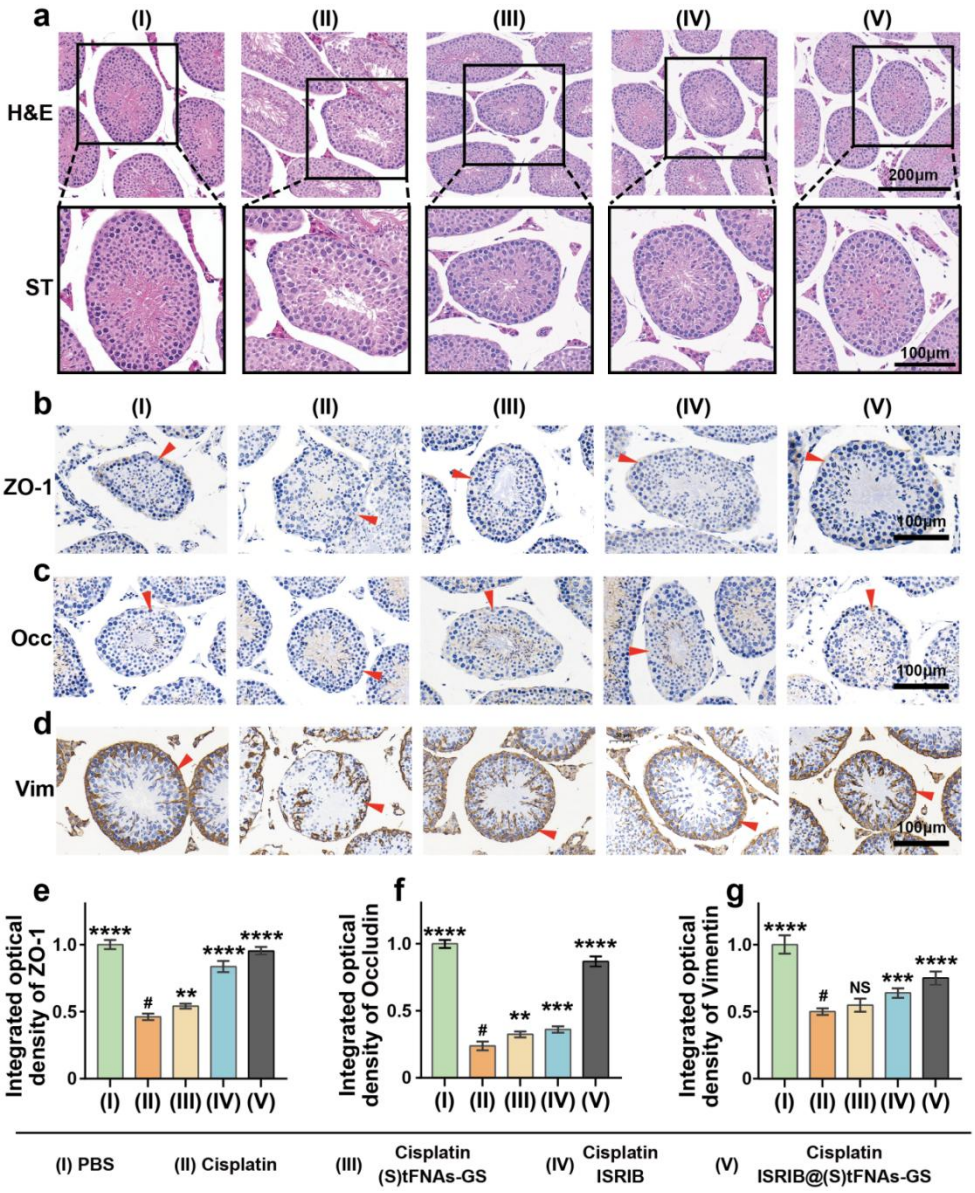


Figure 8. *In vivo* evaluation of ISRIB@(S)tFNAs-GS for preserving blood–testis barrier integrity and alleviating testicular inflammation. (a) H&E-stained images of seminiferous tubule damage for assessment of the protective capacity of ISRIB@(S)tFNAs-GS after different treatments. (b,e) Representative immunohistochemical images and quantitative data for ZO-1 in the testis. (c,f) Representative immunohistochemical images and quantitative data for Occludin in testicular tissue. (d,g) Representative immunohistochemical images and quantitative data for Vimentin in sertoli cells, displaying cytoskeletal disorganization. # for comparisons between groups, NS: no significant, **P < 0.01, ***P < 0.001.

3. Conclusion

This study presents a DNA nanotechnology-based platform for BTB-targeted fertility preservation during prepubertal cisplatin chemotherapy. The key innovations and findings are threefold.

First, GS24 aptamer functionalization confers TfR-mediated testis targeting on tFNAs in a size-dependent manner, with the 13-nm (S)tFNAs-GS construct achieving the greatest BTB enrichment. Systematic *in vivo* biodistribution studies demonstrated that GS24 modification markedly altered the organ distribution of tFNAs, enabling testicular accumulation that was minimal in unmodified constructs. The observed size-dependent targeting performance establishes a design principle for BTB-penetrating nanocarriers that may be extended to other biological barrier systems. Second, transcriptomic profiling identified the ISR pathway and Krt16 as prominent pathological signatures associated with cisplatin-induced Sertoli cell damage. This unbiased discovery approach, different from previous empirical screening methods, provides a rational basis for the selection of ISRIB as the protective agent. The identification of Krt16 as a highly upregulated biomarker offers opportunities for patient stratification and treatment monitoring in future clinical applications. Third, the resulting ISRIB@(S)tFNAs-GS nanoplatform demonstrated excellent physicochemical stability, effective BTB targeting, and significant protective efficacy both *in vitro* and *in vivo*—restoring tight-junction integrity, suppressing Krt16, reducing BTB permeability, and preserving seminiferous tubule architecture. The combination of targeted enrichment and pathway-specific intervention provides a comprehensive strategy to address both drug delivery and efficacy challenges.

This study establishes a novel transcriptome-guided, DNA nanostructure-mediated targeted strategy for chemotherapy-associated reproductive protection. The modular nature of the tFNA platform enables adaptation to other protective agents or targeting ligands, and the noninvasive systemic administration offers significant advantages over conventional techniques. With its excellent biosafety and translational potential, this approach holds promise for further development as a fertility-protection strategy for prepubertal patients receiving cisplatin chemotherapy.

Supplementary Information

The online version contains supplementary material available at https://doi. org/10.XXXX/XXXXXX-XXX-XXXXX-X.

Additional file 1: **Table S1 to S2** and **Figures S1 to S4**

Acknowledgements

Not applicable.

Author contribution

Q. C. Writing original draft, Methodology, Investigation, Conceptualization. **Z. F.** Writing original draft, Validation, Data curation. **K. G.** Methodology, Investigation. **C. F.** Validation, Investigation. **J. L.** Investigation. **L. Y.** Investigation, Data curation. **J. H.** Data curation. **F. Z.** editing, Validation. **S. W.** Supervision, review & editing, Formal analysis. **A. X.** Supervision, Project administration, Funding acquisition.

Funding

The authors thank the financial support of the National Natural Science Foundation of China (No. 82373236, No.82573469, No.82570909), China Postdoctoral Science Foundation (No.2023M741564, No.GZC20240661), President Foundation of Zhujiang Hospital of Southern Medical University (No.yzjj2024qn26), Guangdong Medical Science and Technology Research Foundation (No.A2026128, No.A2024597), Guangzhou Science and Technology Fund Projects (No.SL2023A04J02335), Changzhou's 14th Five-Year Plan for High-Level Health Talent Project (Grant No. 2024BJHB015) and Changzhou ScienceTechnology Program (Grant No. 20220115, No.20259023).

Declarations

Ethics approval and consent to participate

All animal experiments and welfare protocols were strictly conducted in accordance with the guidelines and approval of the Southern Medical University's Institutional Animal Care and Use Committee (Approval numbers: LAEC-2025-014),

Competing interests

The authors declare that they have no competing interests

Data availability

Data will be made available on request.

Consent for publication

All authors of this study agreed to publish.

Author details

[1] Department of Urology, Zhujiang Hospital, Southern Medical University, Guangzhou, 510282, P. R. China.

[2] Department of Pediatric Hematology, Zhujiang Hospital, Southern Medical University, Guangzhou, 510282, P. R. China.

[3] Department of General Section III, Guangdong Provincial Geriatrics Institute, Guangdong Provincial People's Hospital, Guangdong Academy of Medical Sciences, Southern Medical University, Guangzhou, 510080, P. R. China.

[4] Department of Urology, Nanjing First Hospital, Nanjing Medical University, Nanjing, 210006, P. R. China.

[5] Changzhou Maternal and Child Health Care Hospital, Changzhou Medical Center, Nanjing Medical University, Changzhou, 213016, P. R. China.

References:

[1] Chen X, Yang W, Roberts CWM, Zhang J. Developmental origins shape the paediatric cancer genome. ***Nat. Rev. Cancer.*** **2024**;24:382-398.

[2] Primm KM, Blackman E, Sansbury BM, Zaidi SK, Sengupta R. AACR pediatric cancer progress report 2025. ***Clin. Cancer Res.*** **2026**;32:465-467.

[3] Ni X, Li Z, Liu Y, Bai G, Lu M, Yang Z, Xu X, Zhao W, Cheng KK, Zhang Y, Zheng R, Liu Y, Jia C, Wang X, Wang Y, Shi Q, Yao X, Zhang Y, Su Y, Wang S, Deng Z, Yang W, Duan Y, Zhang R, Wang X, Mao H, Liu S, Li J, Zhang T. Socioeconomic inequalities in cancer survival and access to health care among children and adolescents in China, 2018–24: a prospective nationwide cohort study. ***Lancet.*** **2026**;407:237-255.

[4] Oeffinger KC, Mertens AC, Sklar CA, Kawashima T, Hudson MM, Meadows AT, Friedman DL, Marina N, Kadan-Lottick NS, Schwartz CL, Leisenring W, Robison LL. Chronic health conditions in adult survivors of childhood cancer. ***N. Engl. J. Med.*** **2006**;355:1572-1582.

[5] Katzenstein HM, Malogolovkin MH, Krailo MD, Piao J, Towbin AJ, McCarville MB, Tiao GM, Dunn SP, Langham MR, McGahren ED, Finegold MJ, Ranganathan S, Weldon CB, Thompson PA, Trobaugh-Lotrario AD, O'Neill AF, Furman WL, Chung N, Randazzo J, Rodriguez-Galindo C, Meyers RL. Doxorubicin in combination with cisplatin, 5-flourouracil, and vincristine is feasible and effective in unresectable hepatoblastoma: a Children's Oncology Group study. ***Cancer.*** **2022**;128:1057-1065.

[6] Moke DJ, Luo C, Millstein J, Knight KR, Rassekh SR, Brooks B, Ross CJD, Wright M, Mena V, Rushing T, Esbenshade AJ, Carleton BC, Orgel E. Prevalence and risk factors for cisplatin-induced hearing loss in children, adolescents, and young adults: a multi-institutional North American cohort study. ***Lancet Child***

530 ***Adolesc. Health.*** **2021**;5:274-283.
531 [7] Shaikh F, Stark D, Fonseca A, Dang C, Xia M, Krailo M, Pashankar F, Rodriguez-Galindo C, Olson TA,
532 Nicholson JC, Murray MJ, Amatruda D, Billmire S, Stoneham S, Frazier AL. Outcomes of adolescent
533 males with extracranial metastatic germ cell tumors: a report from the Malignant Germ Cell Tumor
534 International Consortium. ***Cancer.*** **2021**;127:193-202.
535 [8] Chow EJ, Stratton KL, Leisenring WM, Oeffinger KC, Sklar CA, Donaldson SS, Ginsberg JP, Kenney LB,
536 Levine JM, Robison LL, Shnorhavorian M, Stovall M, Armstrong GT, Green DM. Pregnancy after
537 chemotherapy in male and female survivors of childhood cancer treated between 1970 and 1999: a report
538 from the Childhood Cancer Survivor Study cohort. ***Lancet Oncol.*** **2016**;17:567-576.
539 [9] Su HI, Lacchetti C, Letourneau J, Partridge AH, Qamar R, Quinn GP, Reinecke JF, Smith JF, Tesch M,
540 Wallace WH, Wang ET, Loren AW. Fertility preservation in people with cancer: ASCO guideline update.
541 ***J. Clin. Oncol.*** **2025**;43:1488-1515.
542 [10] Zhu H, Wang H, Wang D, Liu S, Sun X, Qu Z, Zhang A, Ye C, Li R, Wu B, Liu M, Gao J. Nme8 is
543 essential for protection against chemotherapy drug cisplatin-induced male reproductive toxicity in mice.
544 ***Cell Death Dis.*** **2024**;15:730.
545 [11] Tharmalingam MD, Matilionyte G, Wallace WHB, Stukenborg JB, Jahnukainen K, Oliver E, Goriely A,
546 Lane S, Guo J, Cairns B, Jorgensen A, Allen CM, Lopes F, Anderson RA, Spears N, Mitchell RT. Cisplatin
547 and carboplatin result in similar gonadotoxicity in immature human testis with implications for fertility
548 preservation in childhood cancer. ***BMC Med.*** **2020**;18:374.
549 [12] Kenney LB, Antal Z, Ginsberg JP, Hoppe BS, Bober SL, Yu RN, Constine LS, van Santen HM, Skinner
550 R, Green DM. Improving male reproductive health after childhood, adolescent, and young adult cancer:
551 progress and future directions for survivorship research. ***J. Clin. Oncol.*** **2018**;36:2160-2168.
552 [13] Oktay KH, Marin L, Titus S. Impact of chemotherapy on the ovarian reserve: are all primordial follicles
553 created equal? ***Fertil. Steril.*** **2022**;117:396-398.
554 [14] Jensen CFS, Dong L, Gul M, Fode M, Hildorf S, Thorup J, Hoffmann E, Cortes D, Fedder J, Andersen
555 CY, Sonksen J. Fertility preservation in boys facing gonadotoxic cancer therapy. ***Nat. Rev. Urol.***
556 **2022**;19:71-83.
557 [15] De Beer E, Goossens E. Testicular tissue transplantation: from animal models to clinical application. ***Hum.***
558 ***Reprod. Open.*** **2026**;2026:hoag035.
559 [16] Fan Q, Sun B, Chao J. Advancements in engineering tetrahedral framework nucleic acids for biomedical
560 innovations. ***Small Methods.*** **2025**;9:e2401360.
561 [17] Yang Z, Shi L, Wang Y, Zhou D, Zhang C, Lin Y. Unveiling the potential of tetrahedral DNA frameworks
562 in clinical medicine: mechanisms, advances, and future perspectives. ***Small.*** **2025**;21:e2410162.
563 [18] Zhang T, Tian T, Lin Y. Functionalizing framework nucleic-acid-based nanostructures for biomedical
564 application. ***Adv. Mater.*** **2022**;34:e2107820.
565 [19] Madhanagopal BR, Zhang S, Demirel E, Wady H, Chandrasekaran AR. DNA nanocarriers: programmed
566 to deliver. ***Trends Biochem. Sci.*** **2018**;43:997-1013.

[20] Liu HJ, Xu P. Strategies to overcome/penetrate the BBB for systemic nanoparticle delivery to the brain/brain tumor. ***Adv. Drug Deliv. Rev.*** **2022**;191:114619.

[21] Mojarad-Jabali S, Farshbaf M, Hemmati S, Sarfraz M, Motasadizadeh H, Shahbazi Mojarrad J, Atyabi F, Zakeri-Milani P, Valizadeh H. Comparison of three synthetic transferrin mimetic small peptides to promote the blood-brain barrier penetration of vincristine liposomes for improved glioma targeted therapy. ***Int. J. Pharm.*** **2022**;613:121395.

[22] Linden E, Abels ER, Solinge TS, Neefjes J, Broekman MLD. Overcoming Barriers in Glioblastoma—Advances in Drug Delivery Strategies. ***Cells.*** **2024**;13:998.

[23] Zhao Y, Zhang H, Cui J, Wang JX, Chen MS, Wang HR, Li XN, Li JL. Ferroptosis is critical for phthalates driving the blood-testis barrier dysfunction via targeting transferrin receptor. ***Redox Biol.*** **2023**;59:102584.

[24] Lu HJ, Koju N, Sheng R. Mammalian integrated stress responses in stressed organelles and their functions. ***Acta Pharmacol. Sin.*** **2024**;45:1095-1114.

[25] Costa-Mattioli M, Walter P. The integrated stress response: from mechanism to disease. ***Science.*** **2020**;368:eaat5314.

[26] Lawrence RE, Shoemaker SR, Deal A, Sangwan S, Anand AA, Wang L, Marqusee S, Walter P. A helical fulcrum in eIF2B coordinates allosteric regulation of stress signaling. ***Nat. Chem. Biol.*** **2024**;20:422-431.

[27] Chandrasekaran AR. Nuclease resistance of DNA nanostructures. ***Nat. Rev. Chem.*** **2021**;5:225-239.

[28] Shi S, Li Y, Zhang T, Xiao D, Tian T, Chen T, Zhang Y, Li X, Lin Y. Biological effect of differently sized tetrahedral framework nucleic acids: endocytosis, proliferation, migration, and biodistribution. ***ACS Appl. Mater. Interfaces.*** **2021**;13:57067-57074.

[29] Liang L, Li J, Li Q, Huang Q, Shi J, Yan H, Fan C. Single-particle tracking and modulation of cell entry pathways of a tetrahedral DNA nanostructure in live cells. ***Angew. Chem. Int. Ed.*** **2014**;53:7745-7750.

[30] Zhu S, Peng H, Kong H, Yan Q, Xia K, Wang L, Zhu Y, Luo S. Visualization of the hepatic and renal cell uptake and trafficking of tetrahedral DNA origami in tumour. ***Cell Prolif.*** **2024**;57:e13643.

[31] Jiang D, Ge Z, Im HJ, England CG, Ni D, Hou J, Zhang L, Kutyreff CJ, Yan Y, Liu Y, Cho SY, Engle JW, Shi J, Huang P, Fan C, Yan H, Cai W. DNA origami nanostructures can exhibit preferential renal uptake and alleviate acute kidney injury. ***Nat. Biomed. Eng.*** **2018**;2:865-877.

[32] Huang Y, Ning X, Ahrari S, Cai Q, Rajora N, Saxena R, Yu M, Zheng J. Physiological principles underlying the kidney targeting of renal nanomedicines. ***Nat. Rev. Nephrol.*** **2024**;20:354-370.

[33] Cannarella R, Curto R, Condorelli RA, Lundy SD, La Vignera S, Calogero AE. Molecular insights into Sertoli cell function: how do metabolic disorders in childhood and adolescence affect spermatogonial fate? ***Nat. Commun.*** **2024**;15:5582.

[34] Liu X, Wang X, Zhang X, Zhang Y, Gong B, Zhu P, Liu F. Human umbilical cord mesenchymal stem cells ameliorates cisplatin-induced blood-testis barrier dysfunction in mice by mitigating ferroptosis. ***Stem Cell Res. Ther.*** **2025**;16:511.

[35] Chiang YF, Chen YT, Huang KC, Hung WL, Chung CP, Shieh TM, Huang YJ, Ali M, Hsia SM. Protective effects of L-cysteine against cisplatin-induced oxidative stress-mediated reproductive damage.

Antioxidants. **2024**;13:1443.

[36] Labbé K, LeBon L, King B, Vu N, Stoops EH, Ly N, Lefebvre AEYT, Seitzer P, Krishnan S, Heo JM, Bennett B, Sidrauski C. Specific activation of the integrated stress response uncovers regulation of central carbon metabolism and lipid droplet biogenesis. ***Nat. Commun.*** **2024**;15:8301.

[37] Nwosu GO, Powell JA, Pitson SM. Targeting the integrated stress response in hematologic malignancies. ***Exp. Hematol. Oncol.*** **2022**;11:94.

[38] Frias ES, Hoseini MS, Krukowski K, Paladini MS, Grue K, Ureta G, Rienecker KDA, Walter P, Stryker MP, Rosi S. Aberrant cortical spine dynamics after concussive injury are reversed by integrated stress response inhibition. ***Proc. Natl. Acad. Sci. U.S.A.*** **2022**;119:e2209427119.

[39] Chou A, Krukowski K, Jopson T, Zhu PJ, Costa-Mattioli M, Walter P, Rosi S. Inhibition of the integrated stress response reverses cognitive deficits after traumatic brain injury. ***Proc. Natl. Acad. Sci. U.S.A.*** **2017**;114:E6420-E6426.

[40] Safarkhani M, Ahmadi S, Ipakchi H, Saeb MR, Makvandi P, Ebrahimi Warkiani M, Rabiee N, Huh Y. Advancements in aptamer-driven DNA nanostructures for precision drug delivery. ***Adv. Sci.*** **2024**;11:2401617.

[41] Chen C, Yu M, Li Q, Zhou Y, Zhang M, Cai S, Yu J, Huang Z, Liu J, Kuang Y, Tang X, Chen W. Programmable tetrahedral DNA-RNA nanocages woven with stimuli-responsive siRNA for enhancing therapeutic efficacy of multidrug-resistant tumors. ***Adv. Sci.*** **2024**;11:2404112.

[42] Ma C, Jiang W, Ma Y, Deng Z, Yuan H, Qian Y, Zhou F, Guo JJ. WYRGRL-functionalized tetrahedral DNA integrates ROS scavenging and miR-26b-5p delivery for cartilage-specific osteoarthritis treatment. ***Chem. Eng. J.*** **2025**;525:170673.

[43] Chen X, He J, Xie Y, Zhang T, Li S, Zhao Y, Hu N, Cai X. Tetrahedral framework nucleic acid nanomaterials reduce the inflammatory damage in sepsis by inhibiting pyroptosis. ***Cell Prolif.*** **2023**;56:e13424.

[44] Sugawara T, Sonoda K, Chompusri N, Noguchi K, Okada S, Furuse M, Wakayama T. Claudin-11 regulates immunological barrier formation and spermatogonial proliferation through stem cell factor. ***Commun. Biol.*** **2025**;8:148.

Supplementary Files

This is a list of supplementary files associated with this preprint. Click to download.

- SuppottingInformation1.docx